Deuteron global optical model potential for energies up to 200 MeV

Yinlu Han, Yuyang Shi, and Qingbiao Shen
China Institute of Atomic Energy, P.O. Box 275(41), Beijing 102413, People's Republic of China
(Received 13 March 2006; revised manuscript received 3 July 2006; published 31 October 2006)

We present a set of new deuteron global phenomenological optical model potential parameters for nuclides in the mass range $12 \leqslant A \leqslant 209$ with incident energies from threshold up to 200 MeV, based on the experimental data of deuteron total reaction cross sections and elastic scattering angular distributions. The extracted deuteron global optical model potential parameters are compared to existing deuteron global optical potential.

DOI: 10.1103/PhysRevC.74.044615 PACS number(s): 24.10.Ht, 25.45.De

I. INTRODUCTION

The optical model has a significant impact on many branches of nuclear reaction physics. The central assumption of that model is that the complicated interaction between an incident particle and a nucleus can be represented by a complex mean-field potential, which divides the reaction flux into a part covering shape elastic scattering and a part describing all competing nonelastic channels. Solving the Schrödinger equation with this complex potential yields a prediction for the basic observables, namely, the elastic scattering angular distribution and total reaction cross sections. An important feature of a good optical model potentials is that it can be used to reliably predict these observables for energies and nuclides for which no experimental measurement data exist, while the ingredients of the model, either microscopic or phenomenological, are physically well-behaved. Moreover, the quality of several derived quantities that are provided by the optical model has an important impact on the evaluation of the various nonelastic channels. Well-known examples are the related transmission coefficients that enter the statistical model of compound nucleus evaporation, and the distorted wave functions that are used for the description of direct inelastic scattering to discrete states as well as in evaluations of multistep direct transitions to the continuum. The reaction cross sections that are calculated with the optical model are important for the evaporation part of intranuclear cascade models and also for semiclassical preequilibrium models. All these nuclear models for the nonelastic channels rely on various other ingredients, such as discrete level schemes, level densities, γ-ray strength functions, fission barriers, etc. Uncertainties in those quantities all add to the total uncertainty of the calculated results. Therefore, it is crucial that the optical model potentials that enter such nuclear model calculations be adequately determined, independent pieces of information. The success of the optical model to account for elastic nucleon scattering and absorption leads to one to apply this model also to composite particle scattering and absorption. It is of special interest to probe the validity of the optical model for the elastic scattering and absorption of deuterons that are weakly bound composite particles.

Most reports on the elastic scattering of deuterons contain one or more optical potentials that reproduce the elastic scattering angular distributions. There are two deuteron global optical model potentials currently available. The first, from Daehnick *et al.* [1], covers the mass range $A = 27$–238. Some ^{12}C and ^{24}Mg data are included at 80 and 90 MeV with reduced weights because not much higher mass data exist at these energies. The full energy range covered is thus 11.8–90.0 MeV. Both relativistic and nonrelativistic forms of the potential were extracted. The other global potential is from Bojowald *et al.* [2]. This potential covers the mass range from $A = 12$–208 and energy range from 52 to 85 MeV. This group took additional data at 58.7 and 85 MeV on several targets, so their data set includes higher energy work. Only nonrelativistic potentials were extracted. Using the extrapolated potential of Bojowald *et al.* and Daehnick *et al.* as a starting point, three improved sets of local optical model potential parameters for C, ^{58}Ni, and ^{208}Pb at incident deuteron energies 110 and 120 MeV, ^{12}C, ^{24}Mg, and ^{58}Ni at incident deuteron energy 170 MeV, ^{6}Li, ^{16}O, ^{32}S, ^{50,51}V, and ^{70,72}Ge at incident deuteron energy 171 MeV and ^{90}Zr and ^{116}Sn at incident deuteron energy 183 MeV were determined by fitting the relevant data [3–5], respectively.

Partial wave analyses of elastic scattering angular distributions result in sets of phase shifts that also uniquely determine the reaction cross sections. In spite of the fact that the analyses of the angular distributions often results in ambiguities for the optical model potential, experimental efforts in the past have mainly concentrated on measuring angular distributions for more target nuclei and at new energies, while up to now very few measurements of total reaction cross sections were only performed in Refs. [6–8].

The purpose of the present paper is to derive a set of global phenomenological optical model potential parameters including the experimental data of deuteron total reaction cross sections and deuteron elastic scattering angular distributions at incident deuteron energy up to 200 MeV.

II. THE OPTICAL MODEL POTENTIAL

The optical model potentials considered here are Woods-Saxon form for the real part; Woods-Saxon and derivative Woods-Saxon form for the imaginary parts corresponding to the volume and surface absorption, respectively; and the Thomas form for the spin-orbit part. The analytical expression

 ©2006 The American Physical Society

of the phenomenological optical model potential form is

$$V(r) = V_R(r) + V_{SO}(r) + V_C(r) + i[W_D(r) + W_S(r) + W_{SO}(r)], \quad (1)$$

where $V_R(r)$ is the real part potential, $W_D(r)$ and $W_S(r)$ are the imaginary part potential of surface absorption and volume absorption, $V_{SO}(r)$ and $W_{SO}(r)$ are the real and imaginary parts of the spin-orbit potential, $V_C(r)$ is the Coulomb potential. The real part of optical model potential is

$$V_R(r) = -\frac{V_R(E)}{1 + \exp\left(\frac{r-R_R}{a_R}\right)}. \quad (2)$$

The imaginary part of surface absorption of optical model potential is

$$W_D(r) = -4W_D(E)\frac{\exp\left(\frac{r-R_D}{a_D}\right)}{\left[1 + \exp\left(\frac{r-R_D}{a_D}\right)\right]^2}. \quad (3)$$

The imaginary part of volume absorption of optical model potential is

$$W_S(r) = -\frac{W_S(E)}{1 + \exp\left(\frac{r-R_S}{a_S}\right)}. \quad (4)$$

The spin-orbit potential is

$$V_{SO}(r) = -\left(\frac{\hbar}{m_\pi c}\right)^2 (\vec{L}\cdot\vec{S})\frac{V_{SO}}{a_{SO}r}\frac{\exp\left(\frac{r-R_{SO}}{a_{SO}}\right)}{\left[1 + \exp\left(\frac{r-R_{SO}}{a_{SO}}\right)\right]^2}, \quad (5)$$

$$W_{SO}(r) = -\left(\frac{\hbar}{m_\pi c}\right)^2 (\vec{L}\cdot\vec{S})\frac{W_{SO}}{a_{SO}r}\frac{\exp\left(\frac{r-R_{SO}}{a_{SO}}\right)}{\left[1 + \exp\left(\frac{r-R_{SO}}{a_{SO}}\right)\right]^2}. \quad (6)$$

The Coulomb potential is

$$V_C(r) = \begin{cases} 0.7720448\frac{Z_d Z}{R_C}\left(3 - \frac{r^2}{R_C^2}\right) & \text{if } r < R_C, \\ 1.440975\frac{Z_d Z}{r} & \text{if } r \geqslant R_C. \end{cases} \quad (7)$$

The energy dependencies of potential depths are expressed as follows:

$$V_R(E) = V_0 + V_1 E + V_2 E^2 + V_3\frac{(N-Z)}{A} + V_4 Z A^{-\frac{1}{3}}, \quad (8)$$

$$W_D(E) = W_0 + W_1 E + W_2\frac{(N-Z)}{A}, \quad (9)$$

$$W_S(E) = \max\left\{0,\ U_0 + U_1 E + U_2 E^2 + U_3\frac{(N-Z)}{A}\right\}. \quad (10)$$

where Z, N, and A are the charge, neutron, and mass numbers of the target nucleus, respectively, Z_d and E are incident deuteron charge number, and energy in the laboratory system, respectively,

$$R_i = r_i A^{\frac{1}{3}}, \qquad i = R, D, S, SO, C, \quad (11)$$

where r_R, r_D, r_S, r_{SO}, and r_C are the radius of the real part, the surface absorption, the volume absorption, the spin-orbit couple and the Coulomb potential, respectively.

a_R, a_D, a_S, and a_{SO} are the width of the real part, the surface absorption, the volume absorption and the spin-orbit couple potential, respectively. Where a_D, a_S are

$$a_D = a_d + 0.045A^{\frac{1}{3}}, \quad (12)$$

$$a_S = a_s + 0.045A^{\frac{1}{3}}. \quad (13)$$

The units of the potential V_R, W_D, W_S, V_{SO}, W_{SO} are in MeV, the lengths r_R, r_D, r_S, r_{SO}, r_C, a_R, a_D, a_S, and a_{SO} are in fm, the energy E is in MeV.

The Hauser-Feshbach theory with the width fluctuation correction is used to calculate the compound nucleus elastic scattering distributions at low energies.

III. THE GLOBAL OPTICAL MODEL POTENTIAL PARAMETERS

The adjustment of the optical potential parameters is performed automatically with a computer to minimize a quantity called χ^2, which represents the deviation of the calculated results from experimental values. The χ^2 is defined as follows:

$$\chi^2_{i,ne} = \frac{1}{N_{i,ne}}\sum_{j=1}^{N_{i,ne}}\left[\frac{\sigma^{\text{th}}_{i,ne}(j) - \sigma^{\text{exp.}}_{i,ne}(j)}{\Delta\sigma^{\text{exp.}}_{i,ne}(j)}\right]^2, \quad (14)$$

$$\chi^2_{i,el} = \frac{1}{N_{i,el}}\sum_{j=1}^{N_{i,el}}\frac{1}{M_{i,j,el}} \times \sum_{k=1}^{M_{i,j,el}}\left[\frac{\sigma^{\text{th}}_{i,j,el}(\theta_{i,j,k}) - \sigma^{\text{exp.}}_{i,j,el}(\theta_{i,j,k})}{\Delta\sigma^{\text{exp.}}_{i,j,el}(\theta_{i,j,k})}\right]^2, \quad (15)$$

where $N_{i,ne}$ and $N_{i,el}$ are energy point numbers of the experimental data of reaction cross sections, and elastic scattering angular distributions for the ith nucleus, respectively. $M_{i,j,el}$ is angle numbers of the experimental data of elastic scattering angular distributions for the ith nucleus and jth energy point. The superscripts th and exp represent the theoretical and experimental values, respectively. $\sigma_{i,ne}(j)$ are reaction cross sections for the ith nucleus and jth energy point. $\sigma_{i,j,el}(\theta_{i,j,k})$ are elastic scattering angular distributions for the ith nucleus, jth energy point, and kth outgoing angle. $\Delta\sigma$ is the experimental data error of the corresponding data.

The program APMN [9] for automatically searching optimal optical potential parameters in the $E \leqslant 300$ MeV energy range, by means of the improved method of steepest descent [10] is further improved upon and used in the present work.

Starting with the experimental data of total reaction cross sections and elastic scattering angular distributions, we performed the analysis again in order to extract a global parameter set based on as much experimental data as possible. The experimental data of total reaction cross sections and

TABLE I. Optical model potential parameters.

V_0	82.18	V_{SO}	3.703
V_1	−0.148	W_{SO}	−0.206
V_2	−0.000886	r_R	1.174
V_3	−34.811	r_D	1.328
V_4	1.058	r_S	1.563
W_0	20.968	r_{SO}	1.234
W_1	−0.0794	r_C	1.698
W_2	−43.398	a_R	0.809
U_0	−4.916	a_d	0.465
U_1	0.0555	a_s	0.700
U_2	0.0000442	a_{SO}	0.813
U_3	35.0		

elastic scattering angular distributions are collected and analyzed. The nucleus of mass range from $A = 12$–209 and incident deuteron energy range from threshold to 200 MeV are included. The optical model potential parameters obtained is given in Table I.

The real part potential and Coulomb potential of the optical model is used to describe elastic scattering angular distributions. The imaginary part potential of the optical model describes total reaction cross section. From Eqs. (1)–(10) and Table I we can see that the contribution of real part potential [Eqs. (2) and (8)] decreases with increasing incident deuteron energy. The contribution of imaginary part potential of surface absorption [Eqs. (3) and (9)] decreases and imaginary part potential of volume absorption [Eqs. (4) and (10)] increases with increasing incident deuteron energy. The imaginary part potential of volume absorption [Eqs. (4) and (10)] of global optical potential only has contribution for $N \neq Z$ when incident deuteron energy is large about 40.0 MeV. While for $N = Z$, the imaginary part potential of volume absorption [Eqs. (4) and (10)] of global optical potential only has contribution when incident deuteron energy is large about 100.0 MeV. The contribution of the spin-orbit potential [Eqs. (5) and (6)] of the optical model is small.

IV. THEORETICAL CALCULATIONS AND ANALYSIS

The total reaction cross section for ^{12}C, ^{16}O, ^{28}Si, ^{40,48}Ca, ^{58,60}Ni, ^{112,116,120,124}Sn, and ^{208}Pb are calculated using the global optical model potential parameters from Table I. The comparisons of calculated results with experimental data [8] are given in Figs. 1–4. The calculated results show that theoretical values are in good agreement with experimental data [8] for ^{16}O, ^{28}Si, and ^{208}Pb in Fig. 1, and theoretical values are larger than the experimental data [6] for ^{12}C. The calculated results for ^{40,48}Ca and ^{58,60}Ni are in reasonable agreement with experimental data in Figs. 2 and 3. Figure 4 shows that the theoretical results are in good agreement with experimental data for ^{112,116,120}Sn, while for ^{124}Sn, the theoretical results are larger than experimental data at energies 65.5 and 97.4 MeV, and the experimental data are smaller than the experimental data of ^{120}Sn. Since Figs. 1–4 also show total reaction cross sections increase with increasing the mass number and neutron number of the target nucleus,

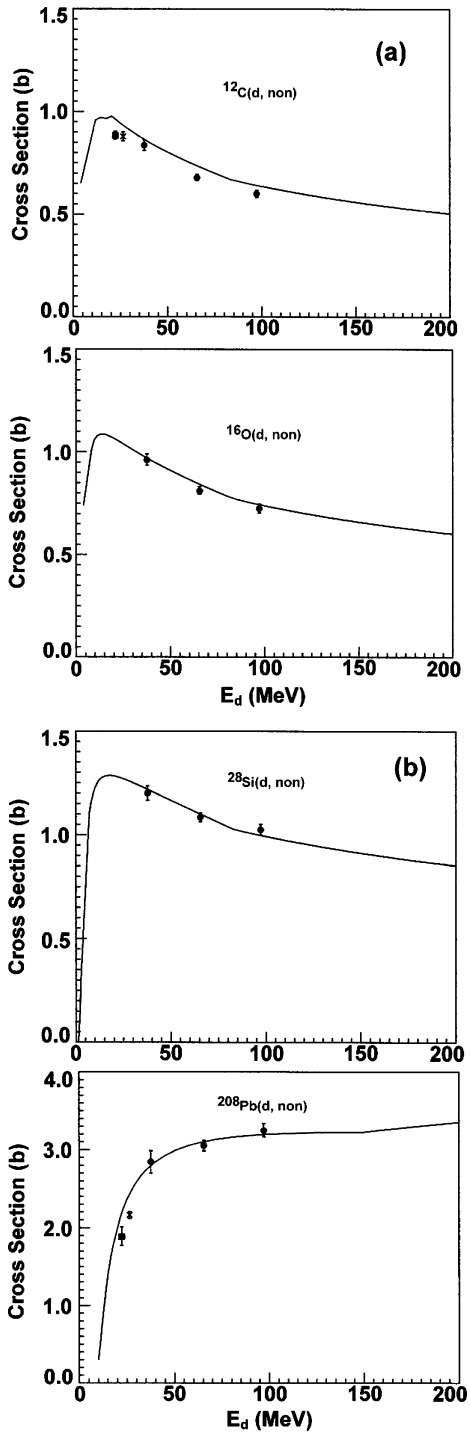

FIG. 1. Experimental data [6–8] of deuteron reaction cross sections for ^{12}C, ^{16}O, ^{28}Si, and ^{208}Pb compared with calculated results by the global potentials.

the theoretical results seem to be reasonable for ^{124}Sn above energies 50 MeV. We also see that there is a general trend that the total reaction cross sections decrease with increasing incident deuteron energy for light nuclei and increase for heavy nuclei. Daehnick *et al.* [1] and Bojowald *et al.* [2] have derived global potentials for the elastic scattering of deuterons below 100 MeV. The difference in the calculated reaction cross

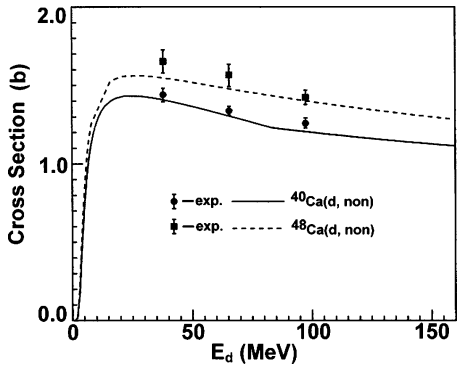

FIG. 2. Experimental data [8] of deuteron reaction cross sections for ^{40}Ca and ^{48}Ca compared with calculated results by the global potentials.

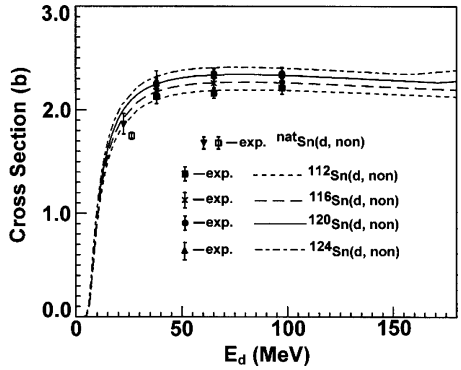

FIG. 4. Experimental data [6–8] of deuteron reaction cross sections for ^{112,116,120,124}Sn compared with calculated results by the global potentials.

sections using these potentials is considerably larger than the experimental data and our present results, and the trend of the total reaction cross sections decreases with increasing energy for all nuclei. It is evident that the total reaction cross sections give a very important constraint on optical model calculations.

The present calculated results of total reaction cross sections for some targets are in agreement with experimental data of natural targets taken from Refs. [6,7] at incident deuteron energies 22.4 and 26.5 MeV, and larger than experimental data of natural targets for some targets as shown in Figs. 1 and 3.

The experimental data of elastic scattering angular distributions in the past have mainly concentrated on measuring for more target nuclei and at new energies. Elastic scattering of the deuteron from Ti, V, Cr, Co, Ni, and Cu at laboratory energies of 3.32 and 4.07 MeV, and from Mg and Al at laboratory energies of 3.32, 3.73, and 4.07 MeV were measured [11]. The calculated results from our global optical potential are in good agreement with experimental data. The comparisons of calculated results with experimental data at incident deuteron energy 4.07 MeV for the elastic scattering angular distributions as a ratio to the Rutherford cross section are given in Fig. 5. There are some structures for ^{24}Mg and ^{27}Al. The present calculated results at incident deuteron energy 9.0 MeV are compared with experimental data [12] for different targets. Except for ^{40}Ca, the present calculated results fit experimental data for all targets. We also calculate and analyze elastic scattering angular distributions of different targets in incident deuteron energy range of 4.0 to 9.0 MeV, the present calculated results are in good agreement with existing experimental data.

The calculated results from our global optical potential as the ratio of differential cross section to the Rutherford cross section at incident deuteron energy 11.0 MeV are compared with experimental data [13] for different targets (^{27}Al to ^{238}U), and good agreement is obtained between present calculated results and experimental data. Elastic scattering angular distributions of deuteron from some natural targets (C to Au), and from some isotope targets (^{27}Al to ^{60}Ni) at laboratory energies of 11.8 MeV were measured [14,15], respectively. Elastic scattering angular distributions of deuteron from different nuclei at laboratory energy of 12.0 MeV were measured [16,17], respectively. There are some discrepancies in both experimental data taken from different laboratories for mass numbers of targets less than 100. The present calculated results are in good agreement with all experimental data for mass numbers of targets

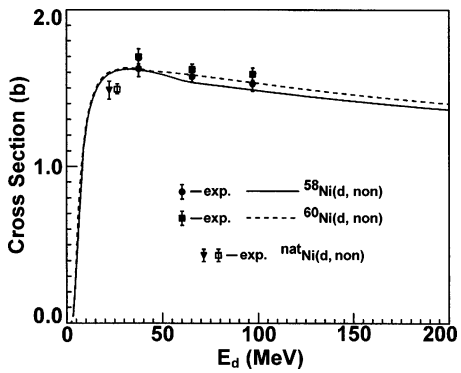

FIG. 3. Experimental data [6–8] of deuteron reaction cross sections for ^{58}Ni and ^{60}Ni compared with calculated results by the global potentials.

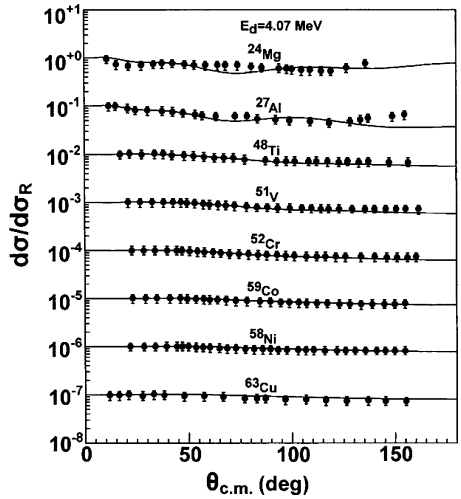

FIG. 5. Elastic scattering angular distributions in the Rutherford ratio at incident deuteron energy of 4.07 MeV compared experimental data [11] with calculated results by the global potentials. The results are offset by factors of 10.

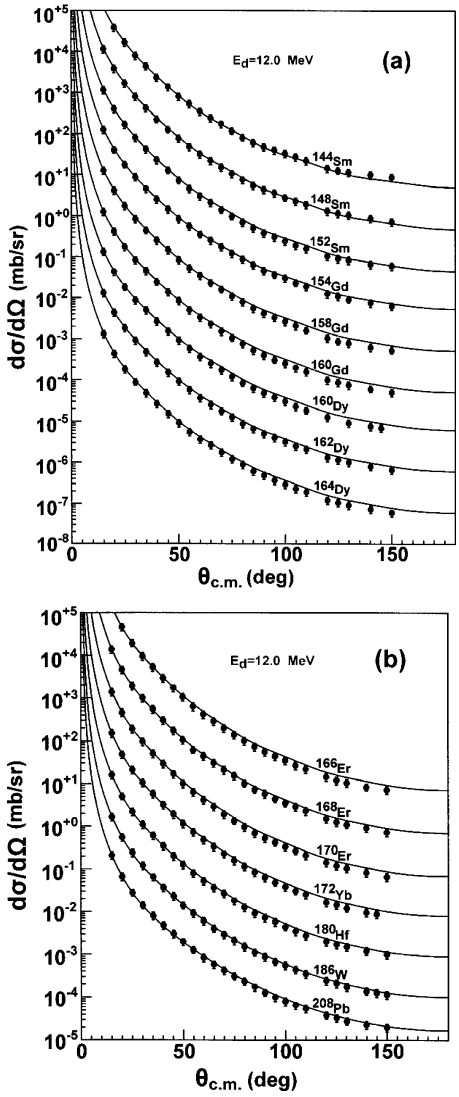

FIG. 6. Elastic scattering angular distributions at an incident deuteron energy of 12.0 MeV compared experimental data [17] with calculated results by the global potentials. The results are offset by factors of 10.

greater than 100. While for mass number of target less than 100, the present calculated results are in agreement with experimental data taken from Refs. [15,16], and are basically in agreement with experimental data taken from Ref. [14]. Figure 6 is the comparisons of present calculated results with experimental data [17] of elastic scattering angular distributions at incident deuteron energy 12.0 MeV. Since Fig. 6 show results for $A > 100$, there are no structure for the shape of elastic scattering angular distributions. While for $A < 100$, since the structure of elastic scattering angular distributions show the nuclear structure effect of the target, the present calculated results of isotope targets are in basically agreement with experimental data of natural targets [14] that are reasonable. The elastic scattering angular distributions of different targets (^{27}Al to ^{208}Pb) at incident deuteron energies 14.5 and 15.0 MeV were measured in different laboratories [18–22]. The measurement results are basically in agreement. The comparisons of present calculated results with all of experimental data [18–22] at incident deuteron energy 15.0 MeV show that a good agreement is obtained. The elastic scattering angular distributions for different targets at incident deuteron energy 17.0 MeV are compared with experimental data [23]. The results show that the present calculated results are in good agreement with experimental data as shown in Fig. 7, except for ^{48}Ca. The experimental data for ^{48}Ca had the larger systematic uncertainty. The present calculated results for ^{12}C and ^{40}Ca are inconsistent with experimental data [13,14] for deuteron energy below 20.0 MeV.

Elastic scattering angular distributions of deuteron from some natural targets (Mg to Au) at incident deuteron energy of 21.6 and 26.0 MeV were measured [24,25]. The calculated results of elastic scattering angular distributions from our global optical potential for the isotope targets corresponding to natural nucleus are compared with all the experimental data. The present calculated results are in good agreement with experimental data. The results at incident deuteron energy 26.0 MeV are only given in Fig. 8.

The calculated results of elastic scattering angular distributions from our global optical potential for ^{12}C, ^{28}Si, ^{40}Ca, ^{56}Fe, ^{58}Ni, ^{64}Zn, ^{90}Zr, ^{118,120}Sn, and ^{208}Pb are compared with experimental data [26,27] at incident deuteron energy about 30.0 MeV. The present calculated results are in good agreement with experimental data, except for ^{12}C and ^{40}Ca, where the shapes of present calculated results curve are similar to those of experimental data, but the magnitudes are smaller than those of experimental data for angle larger 50.0°. The experimental data of elastic scattering angular distributions from different targets at incident deuteron energy of 34.4 MeV were given in Ref. [28]. The present calculated results are in good agreement with experimental data as shown in Fig. 9. From Fig. 9 we can see that the experimental data only were given for angles less than 80°. Since the present calculated results at incident deuteron energy above 30.0 MeV and angle less than 150° are in good agreement with experimental data [26,27], the present calculated results at incident deuteron energy about 34.4 MeV and angle greater than 80° are reasonable.

The comparisons of calculated results from our global optical potential with experimental data [29] of elastic scattering angular distributions at incident deuteron energy 52.0 MeV are given in Fig. 10. The present calculated results are in good agreement with experimental data for some targets, and are in agreement with experimental data for other targets. The experimental data [30] of elastic scattering angular distributions at incident deuteron energy 56 MeV were given. The present calculated results are in good agreement with experimental data for all targets, except ^{16}O, as shown in Fig. 11. The experimental data [31] of elastic scattering angular distributions of deuteron from ^{12}C, ^{16}O, ^{40}Ca, ^{58}Ni, ^{90}Zr, ^{118}Sn, ^{144}Sm, and ^{208}Pb at an incident deuteron energy of 56 MeV were also given. The experimental data taken from Ref. [31] for ^{16}O are inconsistent with those taken from Ref. [30]. The present calculated results are in good agreement with experimental data [31] for all targets. The comparisons of present calculated results with experimental data [2] of elastic scattering angular distributions from ^{27}Al, ^{89}Y, ^{120}Sn,

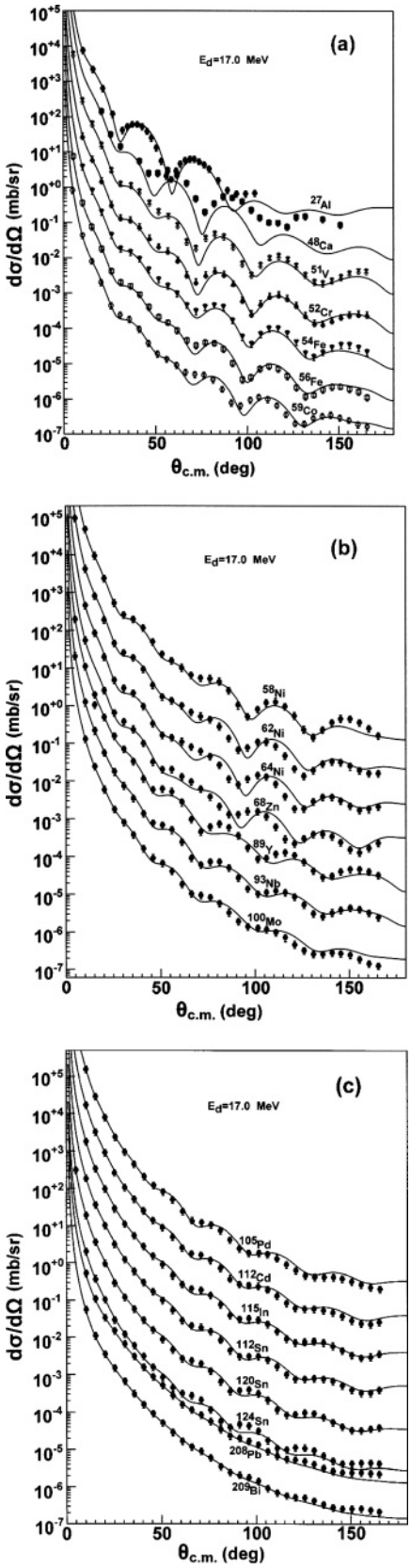

FIG. 7. Elastic scattering angular distributions at an incident deuteron energy of 17.0 MeV compared experimental data [23] with calculated results by the global potentials. The results are offset by factors of 10.

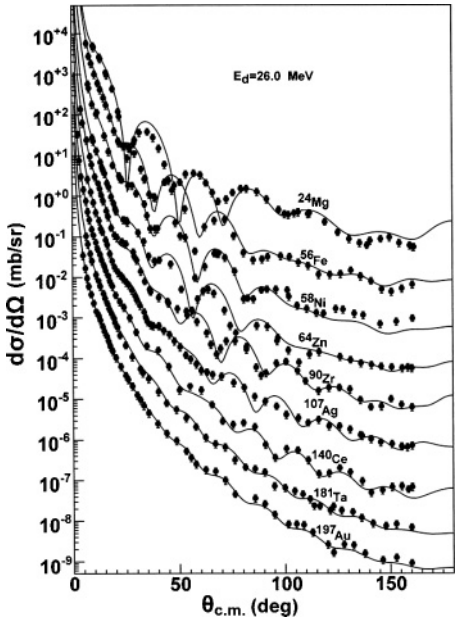

FIG. 8. Elastic scattering angular distributions at an incident deuteron energy of 26.0 MeV compared experimental data [25] with calculated results by the global potentials. The results are offset by factors of 10.

and ^{208}Pb at incident deuteron energy 58.7 MeV are given in Fig. 12. The present calculated results are in good agreement with experimental data for all angles. The agreement between the present calculated results and experimental data in Figs. 10 and 12 show that the present calculated results are reasonable for angles greater than 70° at incident deuteron energy 56 MeV as shown in Fig. 11.

The experimental data of elastic scattering angular distributions at incident deuteron energies 80.0 and 85.0 MeV were given in Refs. [2,32–35], respectively. The comparisons of calculated results from our global optical potential with experimental data show that good agreement is obtained for all targets and energies as shown in Figs. 13 and 14. The present calculated results of elastic scattering angular distributions of ^{12}C, ^{27}Al, ^{58}Ni, and ^{206}Pb at incident deuteron energies 60.0, 77.0, 80.0, 90.0, and 170.0 MeV are compared with experimental data [4,33,34,36]. Comparisons of the present calculated results with experimental data [5] from ^{16}O, ^{32}S, ^{50,51}V, and ^{70,72}Ge at an incident deuteron energy of 171 MeV and from ^{90}Zr and ^{116}Sn at an incident deuteron energy of 183 MeV as ratios of the differential cross section to Rutherford cross section are given in Fig. 15. Though the agreement is obtained between present calculated results and experimental data, the curve of theoretical calculated results shows more diffractive oscillation for angles smaller than 60° above incident deuteron energies of 170 MeV. The elastic scattering angular distributions show a diffraction pattern with weak structure for low energy. The number of diffractive oscillation increases with increasing incident energy. The diffractive oscillation becomes gradually less pronounced with increasing mass number at the same incident energy.

The calculated results of elastic scattering angular distributions from our global optical potentials for the same target

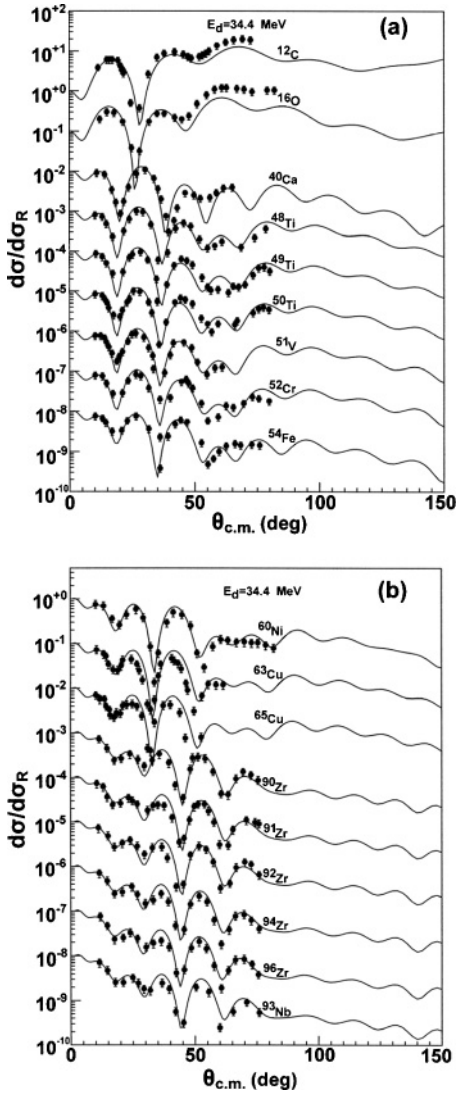

FIG. 9. Elastic scattering angular distributions in the Rutherford ratio at an incident deuteron energy of 34.4 MeV compared experimental data [28] with calculated results by the global potentials. The results are offset by factors of 10.

are compared with experimental data of different incident deuteron energies. Comparisons of the present calculated results with experimental data for ^{24}Mg at incident deuteron energies from 21.0 to 170.0 MeV are given in Fig. 16. The present calculated results are in good agreement with experimental data [4,34]. The experimental data for ^{58}Ni were given at incident deuteron energies from 3.32 MeV to 700.0 MeV [37]. Figure 17 shows the comparisons of present calculated results with experimental data taken from different laboratories for ^{58}Ni at incident deuteron energies from 3.32 to 200.0 MeV. The present calculated results are in good agreement with experimental data. The curve of theoretical calculated results shows more diffractive oscillation for angles smaller than 60° at an incident deuteron energy of 200 MeV. Comparisons of the present calculated results with experimental data for ^{208}Pb at incident deuteron energies from 10.0 to 140.0 MeV are given in Fig. 18. The experimental data

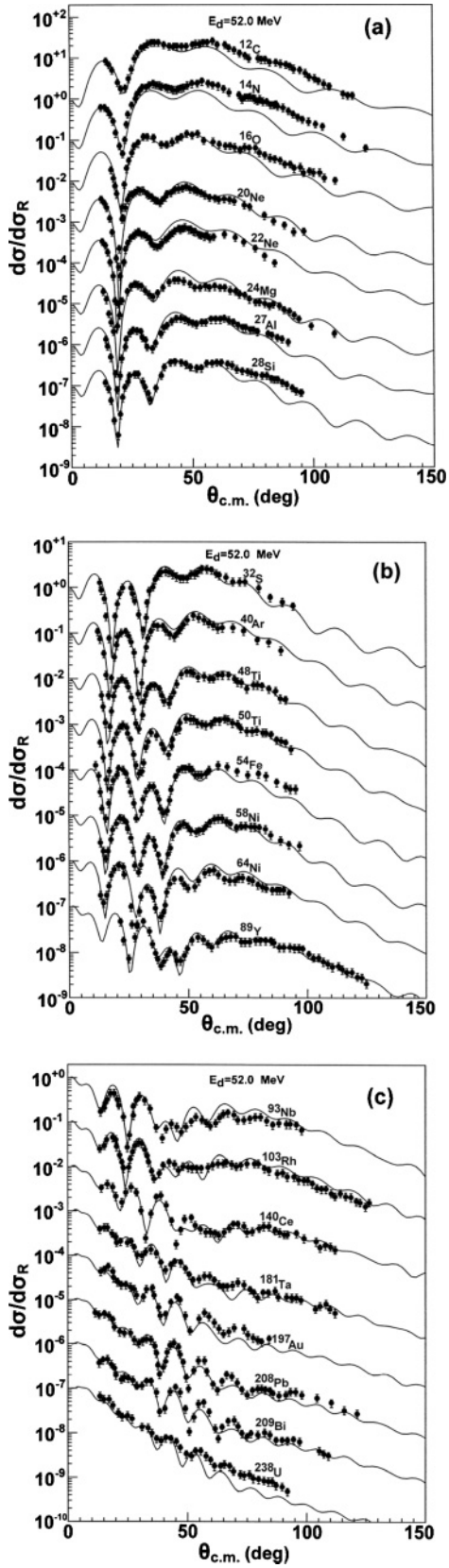

FIG. 10. Elastic scattering angular distributions in the Rutherford ratio at an incident deuteron energy of 52.0 MeV compared experimental data [29] with calculated results by the global potentials. The results are offset by factors of 10.

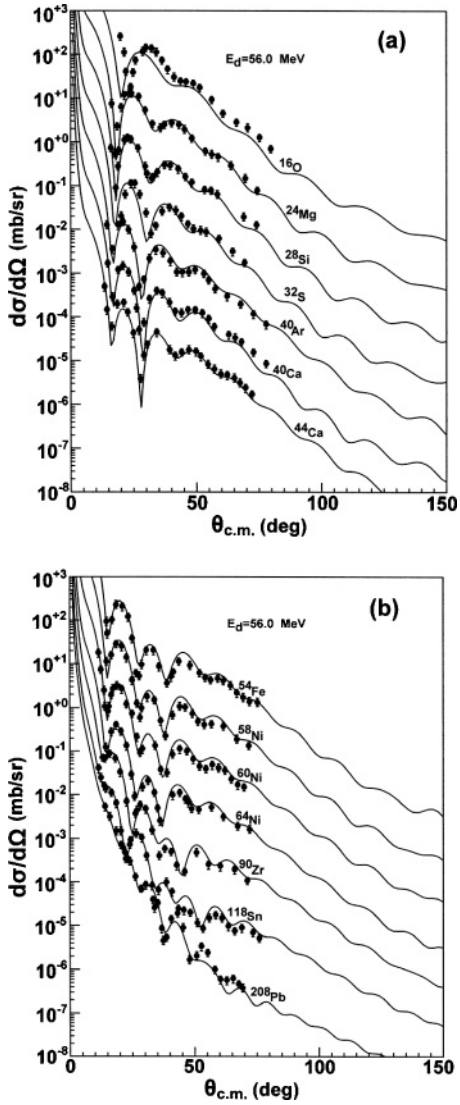

FIG. 11. Elastic scattering angular distributions at an incident deuteron energy of 56.0 MeV compared experimental data [30] with calculated results by the global potentials. The results are offset by factors of 10.

at incident deuteron energies of 10.0, 11.0, 12.0, 13.0, 14.0, 15.0, 16.0, 18.0, 21.5, and 23.0 MeV were given in Ref. [38]. The present calculated results are in good agreement with experimental data for all energy points. The elastic scattering angular distributions show a diffraction pattern with weak structure at larger angles. The first minimum moves to smaller angles with increasing incident energy and becomes gradually less pronounced. The overall slopes of the angular distributions are steeper at higher energies.

The shape of the calculated results curve of elastic scattering angular distributions from our global optical potentials is in good agreement with those of experimental data, but the magnitude is smaller than those of experimental data for ^{12}C and ^{40}Ca below an incident deuteron energy of 40.0 MeV and above an angle of 50°. We also see that the present calculated results of elastic scattering angular distributions for ^{42,44}Ca are in good agreement with those of experimental data, so the

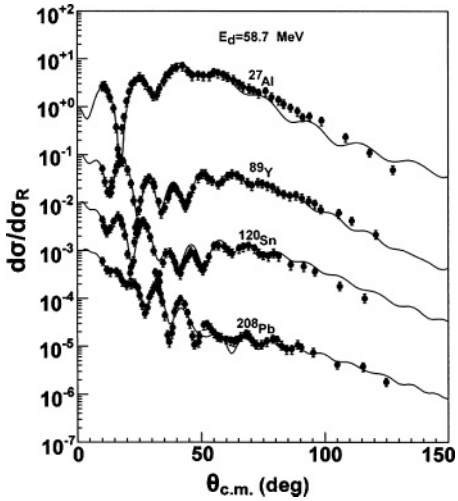

FIG. 12. Elastic scattering angular distributions in the Rutherford ratio at an incident deuteron energy of 58.7 MeV compared experimental data [2] with calculated results by the global potentials. The results are offset by factors of 10.

results for ^{40}Ca show strong nuclear structure effect below an incident deuteron energy of 40.0 MeV. Using our global potential as a starting point, the improved set of local optical model potential parameters for ^{40}Ca at incident deuteron energies of 5.0 to 200 MeV is obtained. The calculated results from our local optical model potential for total reaction cross section and elastic scattering angular distributions are in good agreement with all experimental data. Figure 19 shows the results of elastic scattering angular distributions from our local optical model potential and global optical model potential as well as experimental data [26,39] at incident deuteron energies

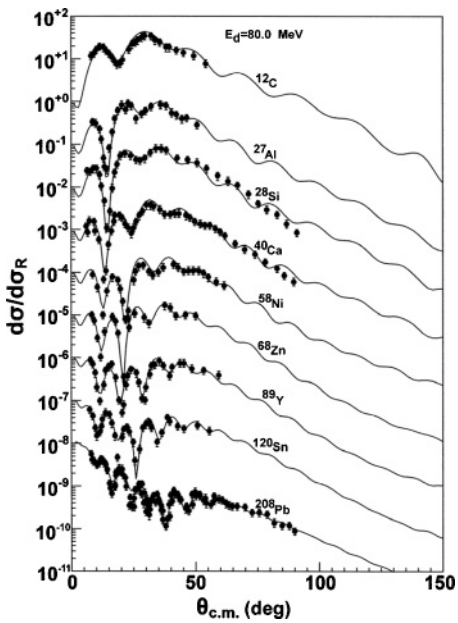

FIG. 13. Elastic scattering angular distributions in the Rutherford ratio at an incident deuteron energy of 80.0 MeV compared experimental data [32–35] with calculated results by the global potentials. The results are offset by factors of 10.

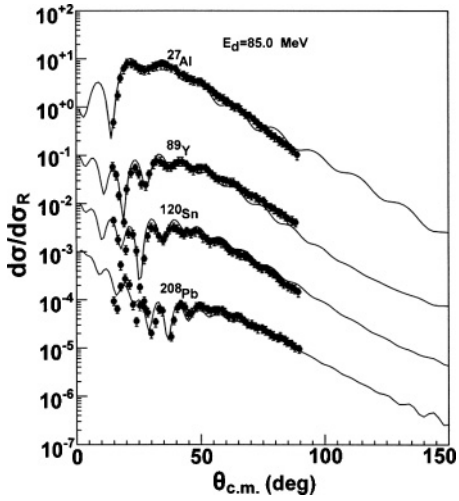

FIG. 14. Elastic scattering angular distributions in the Rutherford ratio at an incident deuteron energy of 85.0 MeV compared experimental data [2] with calculated results by the global potentials. The results are offset by factors of 10.

of 11.18 and 30.0 MeV. The results from our local optical model potential and global optical model potential for elastic scattering angular distributions are in good agreement above an incident deuteron energy of 40.0 MeV, and the total reaction cross sections are in good agreement. The results for ^{12}C are similar to those of ^{40}Ca. The local optical model potential parameters for ^{6,7}Li, ^{9}Be, and ^{10}B will be studied in the future.

The global and local optical model potential parameters for the deuteron were studied for some energy points in the past year, based on the experimental data of elastic scattering

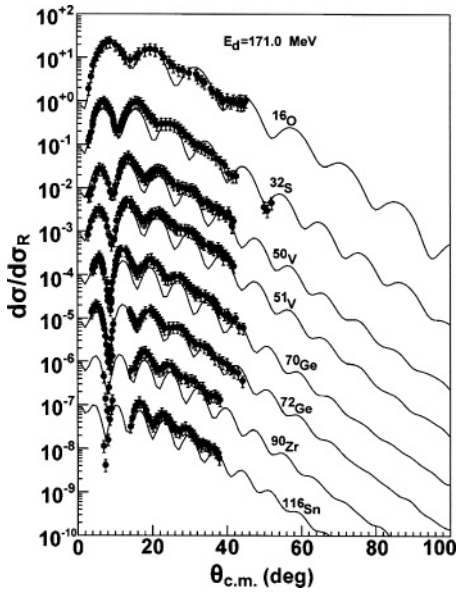

FIG. 15. Elastic scattering angular distributions in the Rutherford ratio at an incident deuteron energies of 171.0 MeV and 183.0 MeV (^{90}Zr and ^{116}Sn) compared experimental data [5] with calculated results by the global potentials. The results are offset by factors of 10.

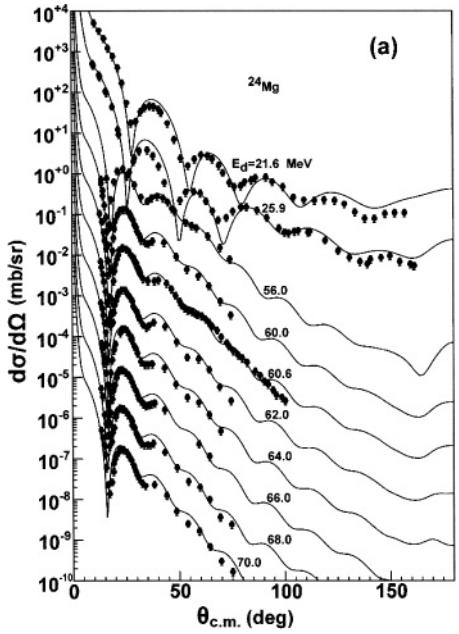

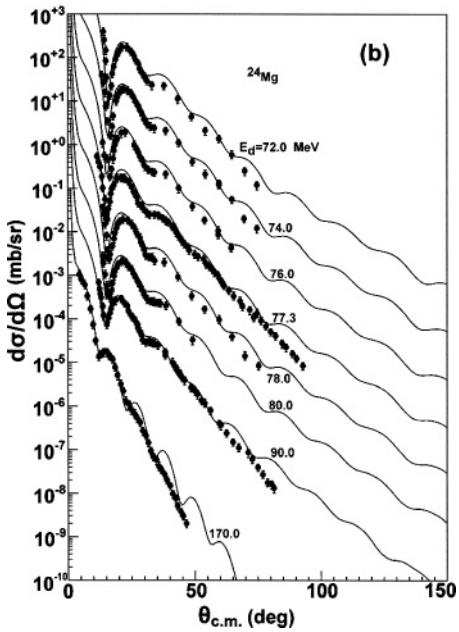

FIG. 16. Elastic scattering angular distributions for ^{24}Mg at different incident deuteron energies compared experimental data [4,34] with calculated results by the global potentials. The results are offset by factors of 10.

angular distributions. Our present work includes all of the experimental data of elastic scattering angular distributions in previous works. The present calculated results improve those from Refs. [1–4].

The global optical model potential parameters for the deuteron were given in Ref. [40]. The energy dependencies of potential depths, the radius and the width of potential are different from our global potentials. Our global potentials include the contribution of the odd-even effect of nuclear structure [the term of $(N - Z)/A$]. The imaginary part of the volume absorption of the optical model potential from

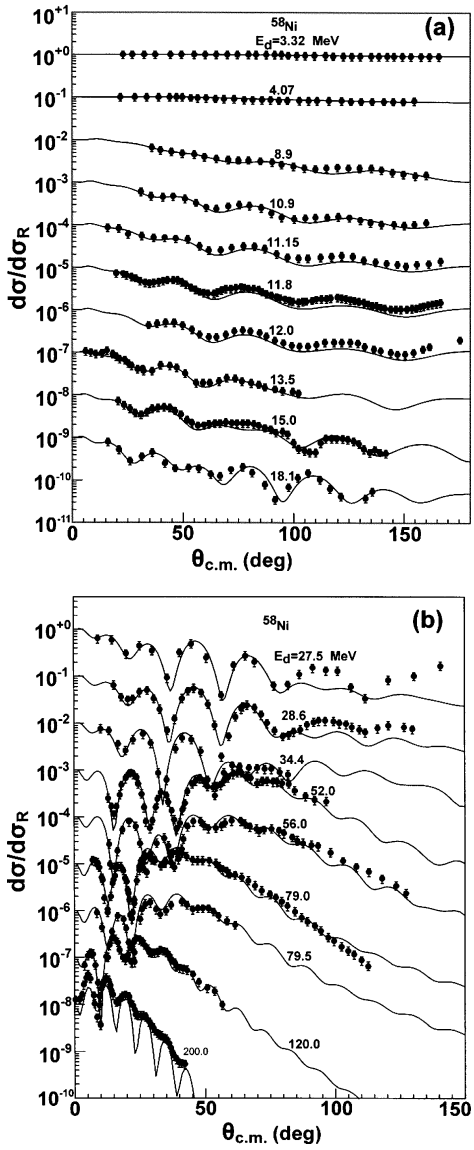

FIG. 17. Elastic scattering angular distributions for ^{58}Ni in the Rutherford ratio at different incident deuteron energies compared experimental data with calculated results by the global potentials. The results are offset by factors of 10.

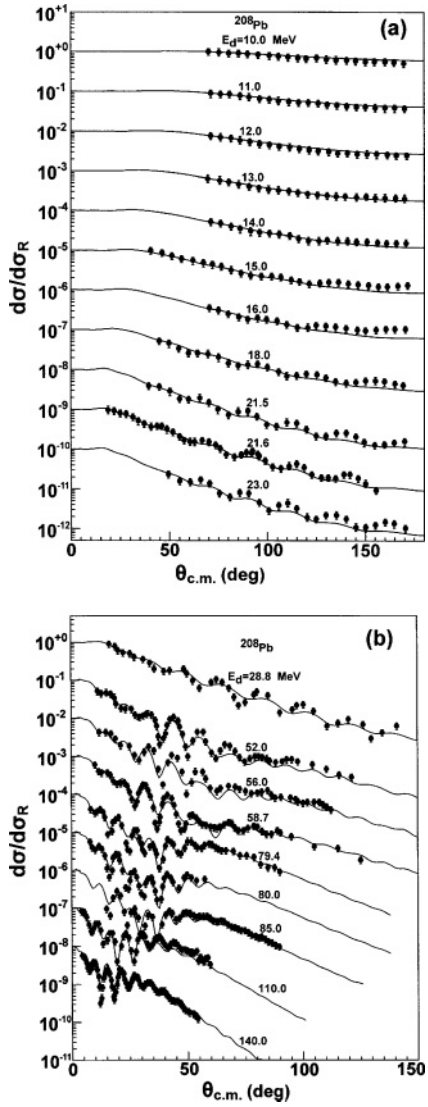

FIG. 18. (a) Elastic scattering angular distributions for ^{208}Pb in the Rutherford ratio at different incident deuteron energies compared experimental data [37] with calculated results by the global potentials. The results are offset by factors of 10. (b) same as (a) but for different experimental data.

Ref. [40] has contributed to all incident deuteron energies, though its value is smaller for low energy. The potentials in Ref. [40] are similar to our potentials with increasing deuteron energy.

Total reaction cross sections have been calculated using the Glauber approach for 20–100 MeV deuterons on targets from ^{9}Be to ^{208}Pb [41,42]. This approximation gives reasonable agreement with the trend of the experimental data. Total reaction cross sections for several targets were calculated for low energy deuterons in the semiclassical approach [43]. For light targets, this approximation gives agreement with experimental data. For Sn and ^{208}Pb, this approximation is inconsistent with the trend of the experimental data for higher energy. The present deuteron global optical model potential overcomes the shortcomings from Refs. [41–43].

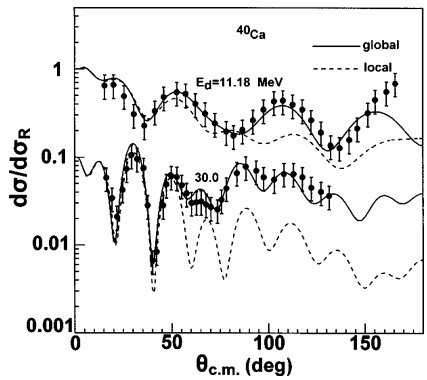

FIG. 19. Elastic scattering angular distributions for ^{40}Ca in the Rutherford ratio at incident deuteron energies 11.18 and 30.0 MeV compared experimental data [26,39] with calculated results by the global potentials and local potentials.

V. CONCLUSIONS

We have reported a set of deuteron global optical model potential parameters for the mass range from 12 to 209 and the energy range from threshold to 200 MeV in this paper, according to the experimental data of deuteron total reaction cross sections and elastic scattering angular distributions. The comparison and analysis of experimental data and calculated results by the global optical model potential show that good agreement is generally observed. The potential developed in this paper may find direct application in theoretical nuclear model calculations and experiment analysis.

ACKNOWLEDGMENTS

This work was done under the Major State Basic Research Development Program of China which is the physical and technological research of the Accelerator-Driven clean nuclear Power System (ADS), and was supported by the China Ministry of Science and Technology under Contract No. G1999022603. This work is a part of IAEA Coordinated Research Projects (CRPs) on Parameters for Calculation of Nuclear Reactions of Relevance to Non-Energy Nuclear Applications under Contract No. 12842/R1.

[1] W. W. Daehnick, J. D. Childs, and Z. Vrcelj, Phys. Rev. C **21**, 2253 (1980).
[2] J. Bojowald, H. Machner, H. Nann, W. Oelert, M. Rogge, and P. Turek, Phys. Rev. C **38**, 1153 (1988).
[3] A. C. Betker, C. A. Gagliardi, D. R. Semon, R. E. Tribble, H. M. Xu, and A. F. Zaruba, Phys. Rev. C **48**, 2085 (1993).
[4] C. Bäumer *et al*., Phys. Rev. C **63**, 037601 (2001).
[5] A. Korff *et al*., Phys. Rev. C **70**, 067601 (2004).
[6] B. Wilkins and G. Igo, Phys. Lett. **3**, 48 (1962).
[7] S. Mayo, W. Schimmerling, M. J. Sametband, and R. M. Eisberg, Nucl. Phys. **62**, 393 (1965).
[8] A. Auce, R. F. Carlson, A. J. Cox, A. Ingemarsson, R. Johansson, P. U. Renberg, O. Sundberg, and G. Tibell, Phys. Rev. C **53**, 2919 (1996).
[9] Q. B. Shen, Nucl. Sci. Eng. **141**, 78 (2002).
[10] B. Alder, S. Fernbach, and M. Rotenberg, Meth. Comput. Phys. **6**, 45 (1966).
[11] I. Slaus and W. Parker Alford, Phys. Rev. **114**, 1054 (1959).
[12] J. M. Lohr and W. Haeberli, Nucl. Phys. **A232**, 381 (1974).
[13] L. D. Knutson and W. Haeberli, Phys. Rev. C **12**, 1469 (1975).
[14] G. Igo, W. Lorenz, and U. Schmidt-Rohr, Phys. Rev. **124**, 832 (1961).
[15] W. Fitz, J. Heger, R. Santo, and S. Wenneis, Nucl. Phys. **A143**, 113 (1970).
[16] H. R. Bürgl, W. Grüebler, J. Nurzynski, V. König, P. A. Schmelzbach, R. Risler, B. Jenny, and R. A. Hardekopf, Nucl. Phys. **A334**, 413 (1980).
[17] P. R. Christensen, A. Berinde, I. Neamu, and N. Scintei, Nucl. Phys. **A129**, 337 (1969).
[18] S. A. Hjorth and E. K. LinA. Johnson, Nucl. Phys. **A116**, 1 (1968).
[19] N. Cindro and N. S. Wall, Phys. Rev. **119**,1340 (1960).
[20] R. K. Jolly, E. K. Lin, and B. L. Cohen, Phys. Rev. **130**, 2391 (1963).
[21] R. P. Goddard and W. Haeberli, Nucl. Phys. **A316**, 116 (1979).
[22] P. W. Keaton Jr., and D. D. Armstrong, Phys. Rev. C **8**, 1692 (1973).
[23] J. D. Childs, W. W. Daehnick, and M. J. Spisak, Phys. Rev. C **C10**, 217 (1974).
[24] J. L. Yntema, Phys. Rev. **113**, 261 (1959).
[25] H. R. E. Tjin A Djie, F. Udo, and L. A. Ch. Koerts, Nucl. Phys. **53**, 625 (1964).
[26] R. Roche, Nguyen Van Sen, G. Perrin, J. C. Gondrand, A. Fiore, and H. Müller, Nucl. Phys. **A220**, 381 (1974).
[27] G. Perrin, Nguyen Van Sen, J. Arvieux *et al*., Nucl. Phys. **A282**, 221 (1977).
[28] E. Newman, L. C. Becker, and B. M. Preedom, Nucl. Phys. **A100**, 225 (1967).
[29] F. Hinterberger, G. Mairle, U. Schmidt-Rohr, G. J. Wagner, and P. Turek, Nucl. Phys. **A111**, 265 (1968).
[30] K. Hatanaka, K. Imai, S. Kobayashi, T. Matsusue, M. Nakamura, K. Nisimura, T. Noro, H. Sakamoto, H. Shimizu, and J. Shirai, Nucl. Phys. **A340**, 93 (1980).
[31] N. Matsuoka *et al*., Nucl. Phys. **A455**, 413 (1986).
[32] G. Duhamel, L. Marcus, H. Langevin-Joliot, J. P. Didelez, P. Narboni, and C. Stephan, Nucl. Phys. **A174**, 485 (1971).
[33] O. Aspelund, G. Hrehuss, A. Kiss, K. T. Knöpfle, C. Mayer-Böricke, M. Rogge, U. Schwinn, Z. Seres, and P. Turek, Nucl. Phys. **A253**, 263 (1975).
[34] A. Kiss, O. Aspelund, G. Hrehuss, K. T. Knöpfle, M. Rogge, U. Schwinn, Z. Seres, P. Turek, and C. Mayer-Böricke, Nucl. Phys. **A262**, 1 (1971).
[35] C. C. Foster, J. C. Collins *et al*., Bull. Am. Phys. Soc. **24**, 594 (1979); **24**, 838 (1979).
[36] M. C. Radhakrishna, N. G. Puttaswamy, H. Nann, J. D. Brown, W. W. Jacobs, W. P. Jones, D. W. Miller, P. P. Singh, and E. J. Stephenson, Phys. Rev. C **37**, 66 (1988).
[37] N. V. Sen *et al*., Phys. Lett. **B156**, 185 (1985).
[38] T. Murayama, Y. Tagishi, T. Sakai, M. Tomizawa, H. Nishikawa, and S. Seki, Nucl. Phys. **A486**, 261 (1988).
[39] M. Takeda, J. Phys. Soc. Jpn. **15**, 557 (1960).
[40] H. An and C. Cai, Phys. Rev. C **73**, 054605 (2006).
[41] R. E. Warner, M. H. McKinnon, H. Thirumurthy, and A. Nadasen, Phys. Rev. C **59**, 1215 (1999).
[42] J. S. al-Khalili and J. A. Tostevin, Phys. Rev. Lett. **76**, 3903 (1996).
[43] R. A. Rego and B. V. Carlson, Phys. Rev. C **66**, 014611 (2002).